

Topological quantum transition driven by charge-phonon coupling in higher-order topological insulators

Congwei Lu,¹ Mei Zhang,¹ Haibo Wang,¹ Qing Ai,¹ and Tao Liu^{2,*}

¹*Department of Physics, Applied Optics Beijing Area Major Laboratory,
Beijing Normal University, Beijing 100875, China*

²*School of Physics and Optoelectronics, South China University of Technology, Guangzhou 510640, China*
(Dated: March 28, 2023)

We investigate a second-order topological quantum transition of a modified Kane-Mele model driven by electron-phonon interaction. The results show that the system parameters of the bare modified Kane-Mele model are renormalized by the electron-phonon interaction. Starting from the second-order topological phase for the bare model, the increasing electron-phonon coupling strength can drive the second-order topological insulator into a semimetal phase. Such a second-order topological phase transition is characterized by the band-gap closing, discontinuity of averaged fermionic number and topological invariant.

I. INTRODUCTION

The past years have witnessed considerable interests and rapid developments in studying higher-order topological insulators (HOTIs)^{1–26}. The hallmark of HOTIs is the existence of topologically-protected boundary states with their dimension at least two lower than the bulk states. Such unconventional boundary states have been experimentally observed in a variety of platforms, including electrical circuits^{7,27–29}, acoustic^{13,14,30,31} and photonic waveguides^{32–34}, phononic metamaterials⁸, and solid-state materials¹⁶. Furthermore, the unconventional bulk-boundary correspondence in HOTIs, with the interplay of disorder^{35–37}, quasicrystal^{19,38,39} and amorphous^{40,41} structures, many-body interactions^{42–44}, non-Hermiticity^{45–47} or periodic driving^{48–54}, has led to many intriguing features uncovered in conventional topological insulators.

Up to now, much effort has been devoted to understanding the effects of disorders^{35–37} and electron-electron interactions^{42–44} on the higher-order topological properties. In contrast, the inevitable roles played by the electron-phonon interaction in solid-state materials remain mostly unexplored in HOTIs. Therefore, it is of interest to address this issue. In conventional first-order topological phases, the electron-phonon interaction has been proven to modify the topological properties of an electronic structure, and induce novel topological phase transitions and robust edge states^{55–62}. One may wonder how the an electron-phonon interaction modifies the topological properties in HOTIs, and whether a higher-order topological phase occurs by tuning the phononic degrees of freedom.

In this paper, we aim to reveal the role played by the electron-phonon coupling of solid-state materials in determining the higher-order topological phase transitions. To be specific, we investigate an Holstein model by introducing the electron-phonon interaction into the modified Kane-Mele model⁶³. The renormalization of the system's parameters due to the electron-phonon coupling is demonstrated by using the Lange-Firsov

approach⁶⁴ in high-frequency limit of the optical phonon mode. Then we employ the cluster perturbation theory to calculate the one-electron spectral function defined via the system's Green's function. We compute the renormalized parameters, band gaps, and energy bands as the electron-phonon coupling strength varies. The electron-phonon interaction modifies the system's parameters, and therefore the band gap closes at the critical electron-phonon coupling strength. These indicate that a topological phase transition occurs. Such a phase transition is further verified by analyzing the fermionic number discontinuity at the critical electron-phonon coupling strength. By calculating the topological invariant, we verify a second-order topological phase transition driven by the electron-phonon coupling.

The rest of the paper is structured as follows. In Sec. II, we review the bare modified Kane-Mele model and its topological phase regimes. In Sec. III, we introduce the Lang-Firsov approach to predict the renormalized parameters, and utilize the cluster perturbation theory to calculate the spectral function and second-order topological phase transitions. The numerical results are presented in Sec. IV. Finally, we conclude the work in Sec. V.

II. THE MODEL WITH CHARGE-PHONON COUPLING

In order to uncover the effects of electron-phonon interactions on the higher-order topological properties, we consider the modified Kane-Mele model⁶³ for spinful electrons in the presence of intrinsic spin-orbit coupling and an in-plane Zeeman field in a honeycomb lattice. Its tight-binding Hamiltonian is written as⁶³

$$\mathcal{H}_0 = -t \sum_{\langle ij \rangle} c_i^\dagger c_j + it_{\text{so}} \sum_{\langle\langle ij \rangle\rangle} \nu_{ij} c_i^\dagger s_z c_j + \lambda \sum_i c_i^\dagger s_y c_i, \quad (1)$$

where $c_i^\dagger = (c_{i\uparrow}^\dagger, c_{i\downarrow}^\dagger)$, with $c_{i\sigma}^\dagger$ ($\sigma = \uparrow, \downarrow$) being the creation operator of an electron with spin- σ at the i th

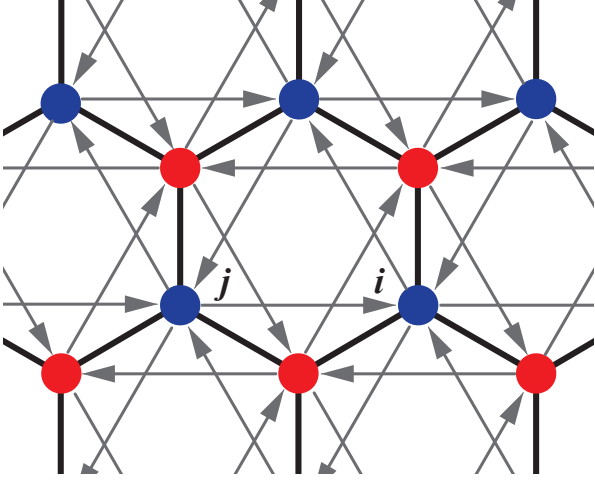


FIG. 1. Schematic of the honeycomb lattice structure. $\nu_{ij} = +1$ when hopping from j to i in the direction of the arrow, otherwise, it has $\nu_{ij} = -1$.

site, s_i ($i = x, y, z$) is the spin-1/2 Pauli matrix, t is the nearest-neighbor hopping amplitude, t_{so} denotes the spin-orbit interaction associated with the next-nearest-neighbor hopping with $\nu_{ij} = \pm$, depending on the hopping direction of the electrons [see Fig. 1(a)], and λ represents the in-plane Zeeman field strength along the y direction. In this paper, we assume $t_{\text{so}} = 0.1t$.

In momentum space by Fourier transforming Eq. (1), we obtain $H_0 = \sum_{\mathbf{k}} \Psi^\dagger \mathcal{H}_0(\mathbf{k}) \Psi$, with

$$\begin{aligned} \mathcal{H}_0(\mathbf{k}) = & \left[t + 2t \cos\left(\frac{3k_y}{2}\right) \cos\left(\frac{\sqrt{3}k_x}{2}\right) \right] \sigma_x + \lambda \sigma_0 s_y \\ & + 2t \sin\left(\frac{3k_y}{2}\right) \cos\left(\frac{\sqrt{3}k_x}{2}\right) \sigma_y \\ & + 4t_{\text{so}} \cos\left(\frac{3k_y}{2}\right) \sin\left(\frac{\sqrt{3}k_x}{2}\right) \sigma_z s_z \\ & - 2t_{\text{so}} \sin\left(\sqrt{3}k_x\right) \sigma_z s_z, \end{aligned} \quad (2)$$

where $\Psi = (c_{A,\mathbf{k},\uparrow}, c_{A,\mathbf{k},\downarrow}, c_{B,\mathbf{k},\uparrow}, c_{B,\mathbf{k},\downarrow})^T$, and σ and s are Pauli matrices acting on the sublattice and spin degrees of freedom, respectively.

The system $\mathcal{H}_0(\mathbf{k})$ in Eq. (2) exhibits distinct topological phases, depending on the Zeeman field λ . In the absence of an in-plane magnetic field (i.e., $\lambda = 0$), $\mathcal{H}_0(\mathbf{k})$ reserves a time-reversal symmetry, and it is a quantum spin Hall insulator characterized by a \mathbb{Z}_2 topological number⁶⁵. This first-order topological phase supports a pair of helical gapless edge modes counterpropagating along the zigzag edge of the lattice. Once we apply the in-plane magnetic field (i.e., $\lambda \neq 0$), the time-reversal symmetry is broken. In this case, a topological phase transition occurs, and the system enters a second-order topological phase regime. In the open boundary condition, the diamond-shaped nanoflake

supports two localized corner modes. These corner modes are protected by the y -mirror symmetry $\mathcal{M}_y = i\sigma_x s_y$ and chiral symmetry. The existence of second-order corner modes is determined by two mirror-graded winding numbers⁶³ of the Hamiltonian $\mathcal{H}_0(k_x, k_y = 0)$, defined in the eigenstate subspaces of the y -mirror symmetry operator along the high-symmetry line with $k_y = 0$.

To be concrete, the system $\mathcal{H}_0(\mathbf{k})$ enters the second-order topological phase regimes for $0 < \lambda/t < 1$. Figures 2(a) and 2(b) show the eigenenergies under open boundary conditions along the y direction, and both x and y directions, respectively. Second-order mid gap bound states exist for $\lambda/t = 0.1$. For $\lambda/t > 1$, the system $\mathcal{H}_0(\mathbf{k})$ shows a topological semimetal phase protected by y -mirror symmetry. When considering only the half filling, it is a topologically trivial semimetal phase for $1 < \lambda/t < 3$, and a trivial insulator for $\lambda/t > 3$.

In order to study the effects of electron-phonon coupling on higher-order topological phases, we couple spinful fermions to the lattice degrees of freedom. The hybrid system is described by the Holstein electron-phonon coupling Hamiltonian⁵⁹

$$H = H_0 + H_{\text{int}}, \quad (3)$$

with

$$H_{\text{int}} = \omega_0 \sum_i d_i^\dagger d_i + g\omega_0 \sum_{i,\sigma} \left(c_{i,\sigma}^\dagger c_{i,\sigma} - \frac{1}{2} \right) (d_i^\dagger + d_i), \quad (4)$$

where d_i^\dagger creates a phonon at site i , ω_0 is the frequency of the optical phonon mode, and g represents the Holstein electron-phonon coupling strength. In this work, we consider the half filling of spinful electrons, and introduce the dimensionless parameter $\alpha = g^2\omega_0/4t$. By changing the value of α , we found that a topological quantum transition from the semimetal phase to the second-order topological insulator phase can occur without changing the parameters of the electronic system.

III. THE THEORETICAL APPROACHES

A. High optical-mode-frequency limit and Lang-Firsov transformation

We first consider a limited case with the phonon-mode frequency ω_0 much larger than the electronic parameters, i.e., $\omega_0 \gg t, t_{\text{so}}, \lambda$, and g . Now, we can analytically demonstrate the hidden physics of topological phase transitions caused by electron-phonon coupling. In the high optical-mode-frequency limit, by applying the Lang-Firsov transformation⁵⁹,

$$H_{\text{LF}} = e^S H e^{-S}, \quad (5)$$

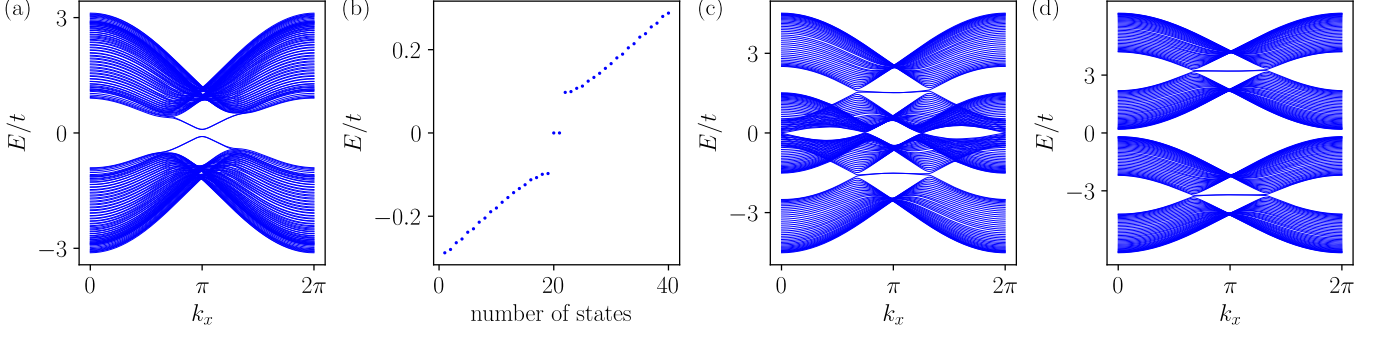


FIG. 2. Band structures under open boundary conditions along the y direction for (a) $\lambda/t = 0.1$, (c) $\lambda/t = 1.5$ and (d) $\lambda/t = 3.2$. (b) Eigenenergies under open boundary conditions along the x and y directions for $\lambda/t = 0.1$.

with

$$S = g \sum_{i,\sigma} \left(c_{i,\sigma}^\dagger c_{i,\sigma} - \frac{1}{2} \right) (d_i^\dagger - d_i), \quad (6)$$

we obtain,

$$H_{\text{LF}} = \tilde{H}_0 + \tilde{H}_{\text{int}}, \quad (7)$$

with

$$\begin{aligned} \tilde{H}_0 = & -t \sum_{\langle ij \rangle} c_i^\dagger c_j X_i^\dagger X_j + it_{\text{so}} \sum_{\langle\langle ij \rangle\rangle} \nu_{ij} c_i^\dagger s_z c_j X_i^\dagger X_j \\ & + \lambda \sum_i c_i^\dagger s_y c_i, \end{aligned} \quad (8)$$

and

$$\tilde{H}_{\text{int}} = \omega_0 \sum_i d_i^\dagger d_i - 2\omega_0 g^2 N_c, \quad (9)$$

where $X_i = e^{g(d_i - d_i^\dagger)}$, and N_c is the number of unit cells.

By considering the thermal average of the phonon modes, we obtain $\langle X_i^\dagger X_j \rangle = e^{-g^2(2N_0+1)}$, where $N_0 = (e^{\beta\omega_0} - 1)^{-1}$, with $\beta = 1/k_B T$, and k_B being the Boltzmann constant. Here we just consider the thermal average of the phonon mode, and neglect its quantum fluctuation $X_i^\dagger X_j - \langle X_i^\dagger X_j \rangle$ for the limited condition $\omega_0 \gg t, t_{\text{so}}, \lambda$ and g . In this antiadiabatic regime, the electronic hopping hardly affects the distribution of phonons, because there exists a larger energy gap between different phonon excitations than the hopping strength of electrons, such that the fast lattice fluctuations make phonon modes immediately follow the charge carriers without modifying their distribution.

Therefore, by rewriting Eq. (8), the parameters t and t_{so} are renormalized as

$$\begin{aligned} \tilde{t} &= t e^{-g^2(2N_0+1)} \\ \tilde{t}_{\text{so}} &= t_{\text{so}} e^{-g^2(2N_0+1)}. \end{aligned} \quad (10)$$

Note that λ in Eq. (8) is not renormalized. In this case, when we tune the electron-phonon coupling strength g , a topological phase transition can occur.

B. Cluster perturbation theory

To numerically solve the electron-phonon coupling in Eq. (3), we calculate the electronic Green function by employing the cluster perturbation theory^{59,64}. The basic idea of the cluster perturbation theory is to divided the infinite lattice into identical clusters, and each cluster contains a finite number of lattice sites. In this case, all the clusters form a superlattice structure with each cluster being an unit cell. In this work, we choose a two-site cluster, containing two nearest-neighbor sublattices, as the unit cell of the superlattice.

We rewrite Eq. (3) as the sum of the cluster Hamiltonian and inter-cluster coupling $H = H_0 + V_{\text{int}}$, with

$$H_0 = \sum_{\mathbf{r}_c} h_0(\mathbf{r}_c), \quad (11)$$

and

$$\begin{aligned} V_{\text{int}} = & -t \sum_{\langle ij \rangle} \sum_{\mathbf{r}_c \neq \mathbf{r}'_c} c_i^\dagger(\mathbf{r}_c) c_j(\mathbf{r}'_c) \\ & + it_{\text{so}} \sum_{\langle\langle ij \rangle\rangle} \sum_{\mathbf{r}_c \neq \mathbf{r}'_c} \nu_{ij} c_i^\dagger(\mathbf{r}_c) s_z c_j(\mathbf{r}'_c), \end{aligned} \quad (12)$$

where $h_0(\mathbf{r}_c)$ reads

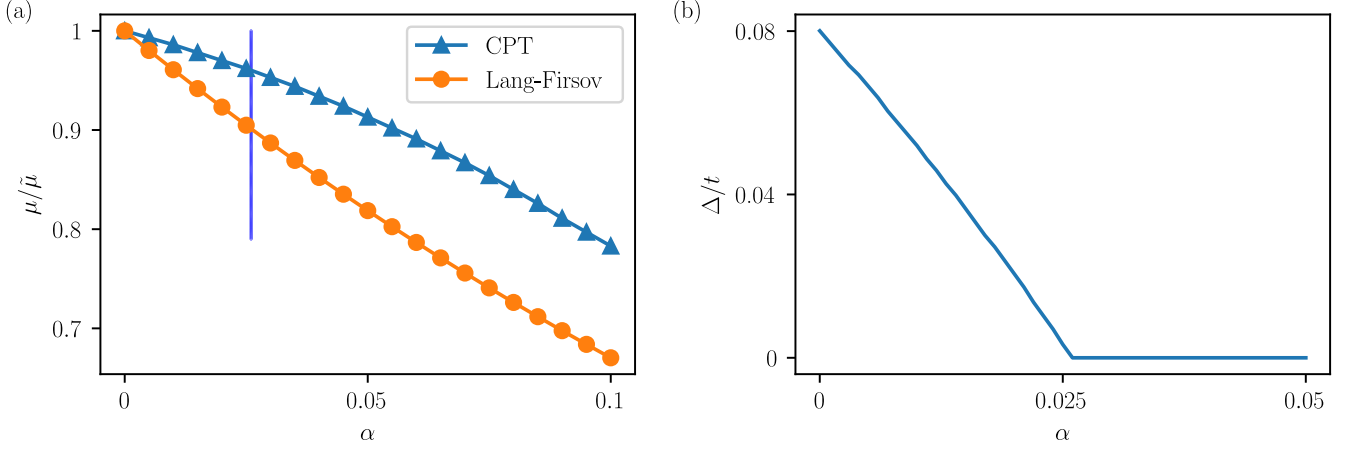


FIG. 3. (a) The renormalized parameters $\mu/\tilde{\mu}$ vs α for the cluster perturbation theory (CPT) and Lang-Firsov approach, respectively. Here, $\mu = \lambda/t$ and $\tilde{\mu} = \tilde{\lambda}/\tilde{t}$. The electron-phonon coupling modifies the system's parameters. The blue vertical line marks the band-gap closing point for $\mu/\tilde{\mu} = 0.96$ and $\tilde{\mu} = 1$ with $\alpha = g^2\omega_0/4t = 0.026$. (b) The renormalized band gap Δ versus α . For $\alpha = 0.026$, the band gap becomes closed, indicating that a topological phase transition occurs.

$$\begin{aligned}
 h_0(\mathbf{r}_c) = & -t \sum_{i \neq j}^2 c_i^\dagger(\mathbf{r}_c) c_j(\mathbf{r}_c) + \lambda \sum_i^2 c_i^\dagger(\mathbf{r}_c) \mathbf{B} \cdot \mathbf{s} c_i(\mathbf{r}_c) + \omega_0 \sum_i d_i^\dagger(\mathbf{r}_c) d_i(\mathbf{r}_c) \\
 & + g\omega_0 \sum_i^2 \left(c_i^\dagger(\mathbf{r}_c) c_i(\mathbf{r}_c) - \frac{1}{2} \right) \left(d_i^\dagger(\mathbf{r}_c) + d_i(\mathbf{r}_c) \right), \quad (13)
 \end{aligned}$$

where $h_0(\mathbf{r}_c)$ is each cluster Hamiltonian, N_c is the number of the clusters, \mathbf{r}_c denotes the site of the center of each cluster, the subscripts i and j denote the sites of the element in each cluster, and V_{int} describes the hopping between clusters.

When employing the cluster perturbation theory, V_{int} is considered as a perturbation to the cluster Hamiltonian H_0 . Therefore, the system Green's function $G(z)$ can be written in terms of the cluster Green's function $\mathcal{G}(z)$ and the perturbation V as

$$G^{-1}(z) = \mathcal{G}^{-1}(z) - V_{\text{int}}, \quad (14)$$

where $z = \omega + i\eta$.

The original lattice has translation symmetry. Therefore, we can Fourier transform, over the whole superlattice, $G^{-1}(z)$ and V in Eq. (14), and achieve

$$G^{-1}(\tilde{\mathbf{k}}, z) = \mathcal{G}^{-1}(z) - V_{\text{int}}(\tilde{\mathbf{k}}), \quad (15)$$

where $\tilde{\mathbf{k}}$ is the wave vector corresponding to the first Brillouin zone of the superlattice, and $\mathbf{k} = \mathbf{k}$ for our case. $\mathcal{G}(z)$ is the retarded cluster Green function at zero

temperature, and it can be written as

$$\begin{aligned}
 \mathcal{G}(z)_{i\sigma, j\sigma'} &= \int dt e^{(i\omega - \eta)t} (-i\theta(t) \langle \Omega | [c_{i\sigma}(t), c_{j\sigma'}^\dagger(0)]_+ | \Omega \rangle) \\
 &= \mathcal{G}_{i\sigma, j\sigma'}^+(z) + \mathcal{G}_{i\sigma, j\sigma'}^-(z), \quad (16)
 \end{aligned}$$

where

$$\mathcal{G}_{i\sigma, j\sigma'}^+(z) = \langle \Omega | c_{i\sigma}(z - h_0 + E_0)^{-1} c_{j\sigma'}^\dagger | \Omega \rangle, \quad (17)$$

$$\mathcal{G}_{i\sigma, j\sigma'}^-(z) = \langle \Omega | c_{i\sigma}^\dagger(z + h_0 - E_0)^{-1} c_{j\sigma'} | \Omega \rangle. \quad (18)$$

In Eqs. (17) and (18), $|\Omega\rangle$ is the ground state of the cluster Hamiltonian h_0 in Eq. (13), and E_0 is the corresponding ground-state energy.

After solving out Eq. (15), the one-electron spectral function can be calculated as

$$A(\tilde{\mathbf{k}}, \omega) = -\frac{1}{\pi} \lim_{\eta \rightarrow 0^+} \text{Im} G(\tilde{\mathbf{k}}, \omega + i\eta), \quad (19)$$

where η can be interpreted as the broadening factor.

IV. NUMERICAL RESULTS

To study the effects of an electron-phonon interaction on the higher-order topological features, we set the

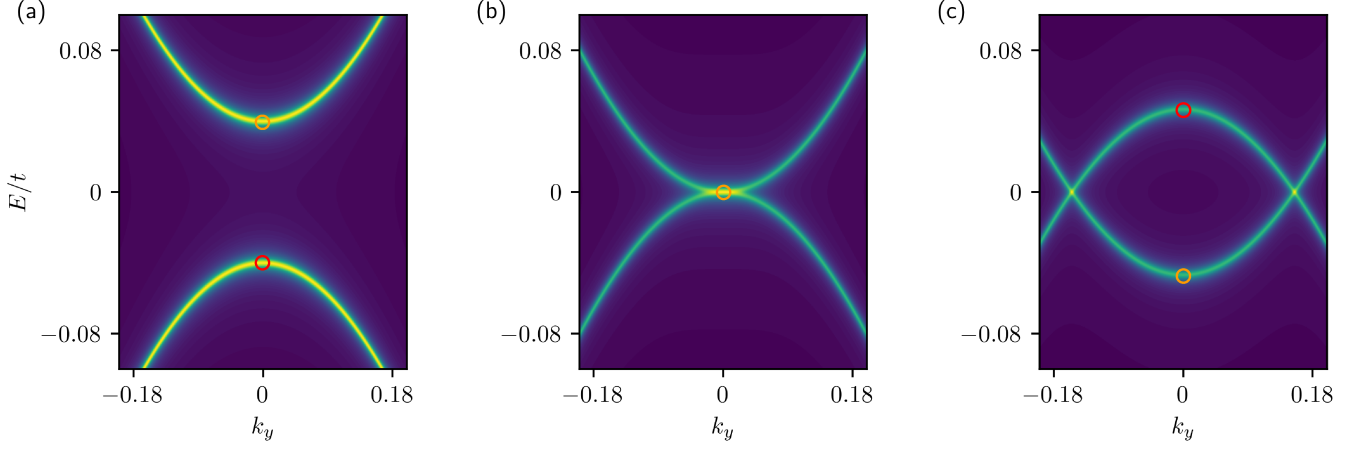


FIG. 4. Energy bands calculated by $\mathcal{H}_{\text{eff}} = -G^{-1}(k_x, k_y, \omega = 0)$ with $k_x = 0$ for (a) $\alpha = 0$, (b) $\alpha = 0.026$, and (c) $\alpha = 0.05$, respectively. A topological phase transition occurs for $\alpha = 0.026$, below which it is an insulator, and becomes a semimetal once $\alpha > 0.026$. Here, we only show the two bands closest to the Fermi level at half filling. The bands marked by red and orange circles are used to calculate the fermionic number. Note that the ground states are not degenerate.

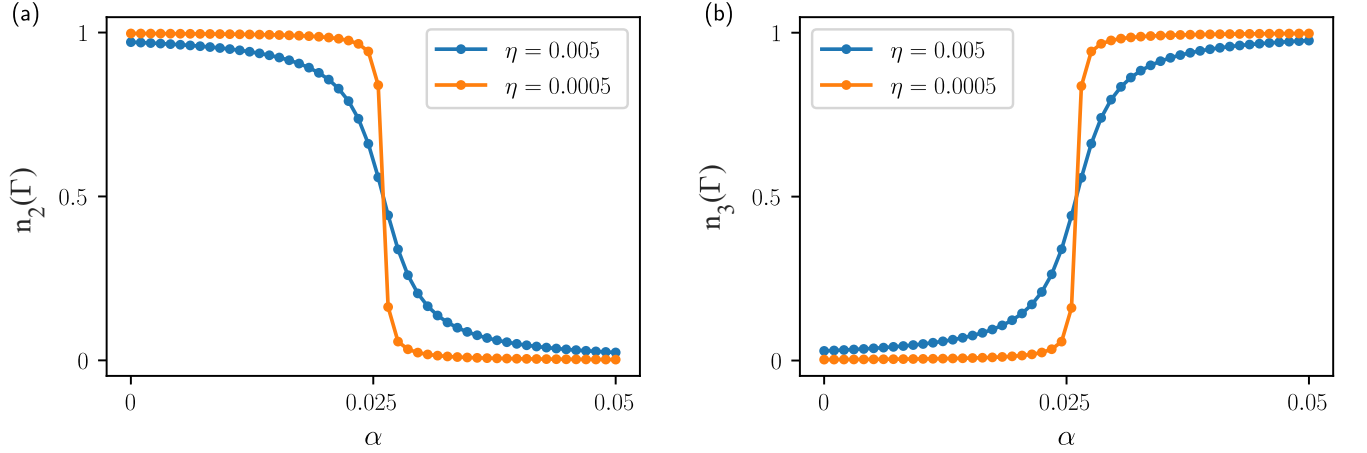


FIG. 5. The average number of fermions $n_2(\Gamma)$ and $n_3(\Gamma)$ for two bands closest to the Fermi level. These two bands initially lie below and above the Fermi energy before the electron-phonon coupling is turned on, and then they pass through the Fermi energy as α increases for different broadening factors η . The subscript here represents the band with the second and third lowest energy when α equals zero.

following parameters, $\omega_0/t = 1$, $t_{\text{so}}/t = 0.1$ and $\lambda/t = 0.96$, where the system, in the absence of electron-phonon coupling, is in the second-order topological phase regime near the phase transition point towards a semimetal phase for half-filling. In this work, we consider only the half-filling case.

As stated above, the Lang-Firsov transformation has shown that the electron-phonon coupling can renormalize system parameters. Furthermore, topological phase regimes are determined by λ/t , as shown in Fig. 2. To reveal the effect of electron-phonon coupling on the system parameters, we plot the ratio of $\mu = \lambda/t$ to the renormalized value $\tilde{\mu} = \tilde{\lambda}/t$ as an introduced dimensionless parameter $\alpha = g^2\omega_0/4t$ varies, as shown

in Fig. 3(a). These results calculated by the cluster perturbation theory are compared with those by the Lang-Firsov approach. As α increases, $\tilde{\mu}$ rises, indicating that the electron-phonon coupling can modify the system's parameters and exhibits the potential for causing the topological phase transitions. In addition, by comparing the results calculated from the Lang-Firsov approach and the ones from the cluster perturbation theory in Fig. 3(a), as the dimensional parameter α increases, the quantum fluctuation of phonon modes starts playing an important role in determining the electronic properties in the large electron-phonon coupling regime.

The topological phase transitions are accompanied by the band-gap closing. In Fig. 3(b), we plot the band

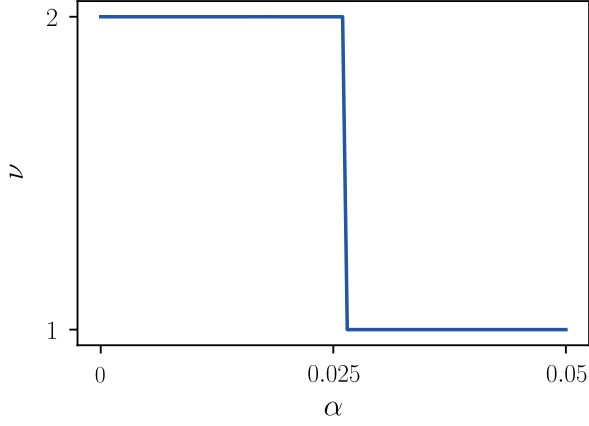


FIG. 6. Winding number $\nu = \nu^- + \nu^+$ vs α . As the α increases, ν changes from 2 ($\nu^\pm = 1$) to 1 ($\nu^+ = 0, \nu^- = 1$), indicating that a second-order topological phase transition occurs.

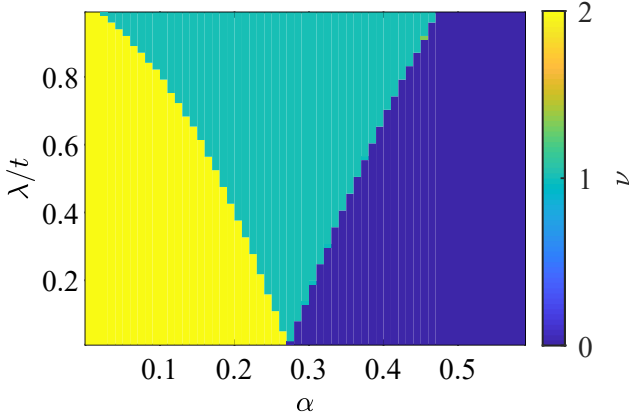


FIG. 7. Phase diagram of the charge-phonon coupling system considered. There exist three phases: a second-order topologically trivial insulator with $\nu = 0$, a semimetal with $\nu = 1$, and a second-order topologically nontrivial insulator with $\nu = 2$.

gaps at half filling versus α . As the α increases, the band gap reduces, and become closed for $\alpha = 0.026$, indicating that a topological phase transition occurs. Furthermore, as shown in Fig. 4, we calculate the band structures of the effective Hamiltonian \mathcal{H}_{eff} , constructed via the full Green's function at zero frequency as $\mathcal{H}_{\text{eff}} = -G^{-1}(k_x, k_y, \omega = 0)$, with $k_x = 0$ for different α , below which it is an insulator, and becomes a semimetal once $\alpha > 0.026$. Here we only show the two bands closest to the Fermi level at half filling. The insulator and semimetal phases are clearly shown, and the phase transition from the insulator to semimetal takes place at $\alpha = 0.026$. Note that the ground states are not degenerate.

To characterize this phase transition, we calculate the average fermionic number n_i of the i th band at Γ point

for half filling as

$$n_i(k_x, k_y) = \int \tilde{A}_{i,i}(k_x, k_y, \omega) n_F(\omega) d\omega, \quad (20)$$

with

$$\tilde{A}(\mathbf{k}, \omega) = \hat{U}^\dagger(\mathbf{k}) A(\mathbf{k}, \omega) \hat{U}(\mathbf{k}), \quad (21)$$

where $\hat{U}(\mathbf{k})$ is a unitary matrix used to diagonalize Hamiltonian $\mathcal{H}_0(\mathbf{k})$ in Eq. (2), and n_F is the Fermi-Dirac distribution. In Fig. 5, we plot $n_2(\Gamma)$ and $n_3(\Gamma)$ as a function of α respectively at zero temperature. The bands, in Fig. 4, marked by a red and orange circles are used to calculate the fermionic number. As α increases, $n_2(\Gamma)$ changes from one to zero, while $n_3(\Gamma)$ varies from zero to one. $n_2(\Gamma)$ and $n_3(\Gamma)$ become discontinuous when we decrease the broadening factor η in Eq. (19) at the phase transition. This discontinuity indicates the topological phase transitions, which can be directly probed.

In order to further determine the second-order topological phase transition, we calculate the topological invariant. The bare modified Kane-Mele model, in the presence of electron-phonon coupling, preserves the y -mirror symmetry. As in the single-particle case⁶³, we calculate the winding number of the effective Hamiltonian $\mathcal{H}_{\text{eff}}(k_x, k_y) = -G^{-1}(k_x, k_y, \omega = 0)$ ⁶⁵ with $k_y = 0$. In the subspace defined y -mirror symmetry, we can rewrite the Hamiltonian \mathcal{H}_{eff} in block diagonal form along the high symmetry line

$$\mathcal{H}_{\text{eff}}(k_x, k_y = 0) = \begin{pmatrix} \mathcal{H}_+(k_x) & 0 \\ 0 & \mathcal{H}_-(k_x) \end{pmatrix}, \quad (22)$$

and then we can define the two mirror-graded winding number

$$\nu^\pm = \int_{-\pi}^{\pi} \frac{dk_x}{4\pi i} \text{Tr} [\tau_z \mathcal{H}_\pm^{-1}(k_x) \partial_{k_x} \mathcal{H}_\pm(k_x)], \quad (23)$$

which can indicate a different phase. Note that quantized winding number is ensured by the chiral symmetry of the system. When the system is in a second-order TI phase, $\nu^\pm = 1$, otherwise it is a second-order topological trivial phase. In our work, we directly calculate $\nu = \nu^- + \nu^+$, which can be written as

$$\nu = \int \frac{dk_x}{4\pi i} \text{Tr} [\tau_0 \otimes \tau_z G(k_x, 0) \partial_{k_x} G^{-1}(k_x, 0)]. \quad (24)$$

If $\nu = 2$, the system is in the second-order topological phase, otherwise it is topologically trivial. In Fig. 6, we plot the winding number as a function of α , which is also discontinuous at $\alpha \simeq 0.026$. This indicates that a second-order topological phase transition occurs at this point. In Fig. 7, we present the phase diagram of the charge-phonon coupling system considered here. There exist three phases: second-order topologically trivial insulator with $\nu = 0$, a semimetal with $\nu = 1$, and a second-order topologically nontrivial insulator with $\nu = 2$. Overall,

the electron-phonon coupling studied in this work can induce higher-order topological phase transitions, and the inevitable roles played by such an electron-phonon interaction should be considered in solid-state materials.

V. CONCLUSION

We have considered a modified Kane-Mele model, which hosts a second-order topological phase for the single-particle case, subjected to electron-phonon coupling. Such a hybrid system is described by the Holstein Hamiltonian, and is solved by using the cluster perturbation approach. We started with the bare modified Kane-Mele model, which is in the second-order topological phase regime in the absence of electron-phonon coupling. When the electron-phonon interaction is turned on, our theoretical calculations on the spectral function via Green's functions show that the band gap becomes closed as the electron-phonon interaction strength increases, and the fermionic number exhibits a finite discontinuity at the transition point at the critical electron-phonon coupling strength. These indicate a topological phase transition. By calculating the topological invariant, the second-order topological phase transition, driven by the electron-phonon coupling, is

verified.

The modified Kane-Mele model can be realized via applying ferromagnetism with in-plane anisotropy⁶³ to topological insulators of silicene⁶⁶ and jacutingaite (Pt_2HgSe_3)⁶⁷, while the electron-phonon coupling may be tuned by the strain or electric field⁶⁸. In addition, the electron-phonon coupling studied here may be simulated using Rydberg states of cold atoms and trapped ions^{69–71}.

ACKNOWLEDGMENTS

T.L. acknowledges the support from National Natural Science Foundation of China (Grant No. 12274142) and the Startup Grant of South China University of Technology (Grant No. 20210012). Q.A. is thankful for the support from Beijing Natural Science Foundation (Grant No. 1202017) and Beijing Normal University (Grant No. 2022129). M.Z. acknowledges the support from the National Natural Science Foundation of China (Grant No. 11475021) and the National Key Basic Research Program of China (Grant No. 2013CB922000). H.B.W. is thankful for the support from National Natural Science Foundation of China (Grant No. 61675028) and National Natural Science Foundation of China (Grant No. 12274037).

* E-mail: liutao0716@scut.edu.cn

- ¹ F. Zhang, C. L. Kane, and E. J. Mele, “Surface state magnetization and chiral edge states on topological insulators,” *Phys. Rev. Lett.* **110**, 046404 (2013).
- ² W. A. Benalcazar, B. A. Bernevig, and T. L. Hughes, “Quantized electric multipole insulators,” *Science* **357**, 61 (2017).
- ³ W. A. Benalcazar, B. A. Bernevig, and T. L. Hughes, “Electric multipole moments, topological multipole moment pumping, and chiral hinge states in crystalline insulators,” *Phys. Rev. B* **96**, 245115 (2017).
- ⁴ J. Langbehn, Y. Peng, L. Trifunovic, F. von Oppen, and P. W. Brouwer, “Reflection-symmetric second-order topological insulators and superconductors,” *Phys. Rev. Lett.* **119**, 246401 (2017).
- ⁵ Z. D. Song, Z. Fang, and C. Fang, “ $(d-2)$ -dimensional edge states of rotation symmetry protected topological states,” *Phys. Rev. Lett.* **119**, 246402 (2017).
- ⁶ F. K. Kunst, G. van Miert, and E. J. Bergholtz, “Lattice models with exactly solvable topological hinge and corner states,” *Phys. Rev. B* **97**, 241405 (2018).
- ⁷ C. W. Peterson, W. A. Benalcazar, T. L. Hughes, and G. Bahl, “A quantized microwave quadrupole insulator with topologically protected corner states,” *Nature* **555**, 346–350 (2018).
- ⁸ M. Serra-Garcia, V. Peri, R. Süssstrunk, O. R. Bilal, T. Larsen, L. G. Villanueva, and S. D. Huber, “Observation of a phononic quadrupole topological insulator,” *Nature* **555**, 342–345 (2018).
- ⁹ M. Geier, L. Trifunovic, M. Hoskam, and P. W. Brouwer, “Second-order topological insulators and superconductors

- with an order-two crystalline symmetry,” *Phys. Rev. B* **97**, 205135 (2018).
- ¹⁰ M. Ezawa, “Higher-order topological insulators and semimetals on the breathing kagome and pyrochlore lattices,” *Phys. Rev. Lett.* **120**, 026801 (2018).
- ¹¹ F. Schindler, A. M. Cook, M. G. Vergniory, Z. J. Wang, S. S. Parkin, B. A. Bernevig, and T. Neupert, “Higher-order topological insulators,” *Science advances* **4**, eaat0346 (2018).
- ¹² X. Zhang, H. X. Wang, Z. K. Lin, Y. Tian, B. Xie, M. H. Lu, Y. F. Chen, and J. H. Jiang, “Second-order topology and multidimensional topological transitions in sonic crystals,” *Nat. Phys.* **15**, 582 (2019).
- ¹³ X. Ni, M. Weiner, A. Alù, and A. B. Khanikaev, “Observation of higher-order topological acoustic states protected by generalized chiral symmetry,” *Nat. Mater.* **18**, 113 (2019).
- ¹⁴ H. Xue, Y. Yang, F. Gao, Y. D. Chong, and B. Zhang, “Acoustic higher-order topological insulator on a kagome lattice,” *Nature materials* **18**, 108–112 (2019).
- ¹⁵ E. Khalaf, “Higher-order topological insulators and superconductors protected by inversion symmetry,” *Phys. Rev. B* **97**, 205136 (2018).
- ¹⁶ F. Schindler, Z. Wang, M. G. Vergniory, A. M. Cook, A. Murani, S. Sengupta, A. Y. Kasumov, R. Deblock, S. J. I. Drozdov, H. Bouchiat, S. Guéron, A. Yazdani, B. A. Bernevig, and T. Neupert, “Higher-order topology in Bismuth,” *Nat. Phys.* **14**, 918 (2018).
- ¹⁷ M. J. Park, Y. Kim, G. Y. Cho, and S. Lee, “Higher-order topological insulator in twisted bilayer graphene,” *Phys. Rev. Lett.* **123**, 216803 (2019).

- ¹⁸ Y. B. Yang, K. Li, L.-M. Duan, and Y. Xu, “Type-II quadrupole topological insulators,” *Phys. Rev. Research* **2**, 033029 (2020).
- ¹⁹ R. Chen, C. Z. Chen, J. H. Gao, B. Zhou, and D. H. Xu, “Higher-order topological insulators in quasicrystals,” *Phys. Rev. Lett.* **124**, 036803 (2020).
- ²⁰ Q. B. Zeng, Y. B. Yang, and Y. Xu, “Higher-order topological insulators and semimetals in generalized Aubry-André-Harper models,” *Phys. Rev. B* **101**, 241104 (2020).
- ²¹ R. Banerjee, S. Mandal, and T. C. H. Liew, “Coupling between exciton-polariton corner modes through edge states,” *Phys. Rev. Lett.* **124**, 063901 (2020).
- ²² Z. R. Liu, L. H. Hu, C. Z. Chen, B. Zhou, and D. H. Xu, “Topological excitonic corner states and nodal phase in bilayer quantum spin hall insulators,” *Phys. Rev. B* **103**, L201115 (2021).
- ²³ C. B. Hua, F. Xiao, Z. R. Liu, J. H. Sun, J. H. Gao, C. Z. Chen, Q. Tong, B. Zhou, and D. H. Xu, “Magnon corner states in twisted bilayer honeycomb magnets,” *arXiv:2202.12151*, 224203 (2022).
- ²⁴ B. Liu, L. D. Xian, H. M. Mu, G. Zhao, Z. Liu, A. Rubio, and Z. F. Wang, “Higher-order band topology in twisted moiré superlattice,” *Phys. Rev. Lett.* **126**, 066401 (2021).
- ²⁵ R. J. Slager, L. Rademaker, J. Zaanen, and L. Balents, “Impurity-bound states and green’s function zeros as local signatures of topology,” *Phys. Rev. B* **92**, 085126 (2015).
- ²⁶ A. K. Ghosh, T. Nag, and A. Saha, “Hierarchy of higher-order topological superconductors in three dimensions,” *Phys. Rev. B* **104**, 134508 (2021).
- ²⁷ S. Imhof, C. Berger, F. Bayer, J. Brehm, L. W. Molenkamp, T. Kiessling, F. Schindler, C. H. Lee, M. Greiter, T. Neupert, *et al.*, “Topological-circuit realization of topological corner modes,” *Nature Physics* **14**, 925–929 (2018).
- ²⁸ M. Serra-Garcia, R. Süssstrunk, and S. D. Huber, “Observation of quadrupole transitions and edge mode topology in an lc circuit network,” *Phys. Rev. B* **99**, 020304 (2019).
- ²⁹ W. X. Zhang, D. Y. Zou, Q. S. Pei, W. J. He, J. C. Bao, H. J. Sun, and X. D. Zhang, “Experimental observation of higher-order topological anderson insulators,” *Phys. Rev. Lett.* **126**, 146802 (2021).
- ³⁰ H. R. Xue, Y. Ge, H. X. Sun, Q. Wang, D. Jia, Y. J. Guan, S. Q. Yuan, Y. D. Chong, and B. Zhang, “Observation of an acoustic octupole topological insulator,” *Nature Communications* **11**, 2442 (2020).
- ³¹ H. Gao, H. R. Xue, Z. M. Gu, T. Liu, J. Zhu, and B. L. Zhang, “Non-hermitian route to higher-order topology in an acoustic crystal,” *Nature Communications* **12** (2019), 10.1038/s41467-021-22223-y.
- ³² S. Mittal, V. Vikram Orre, G. Zhu, M. A. Gorlach, A. Poddubny, and M. Hafezi, “Photonic quadrupole topological phases,” *Nat. Photon.* **13**, 692 (2019).
- ³³ A. E. Hassan, F. K. Kunst, A. Moritz, G. Andler, E. J. Bergholtz, and M. Bourennane, “Corner states of light in photonic waveguides,” *Nature Photonics* **13**, 697–700 (2019).
- ³⁴ M. Li, D. Zhirihin, M. Gorlach, X. Ni, D. Filonov, A. Slobozhanyuk, A. Alù, and A. B. Khanikaev, “Higher-order topological states in photonic kagome crystals with long-range interactions,” *Nat. Photon.* **14**, 89 (2019).
- ³⁵ C. Wang and X. R. Wang, “Disorder-induced quantum phase transitions in three-dimensional second-order topological insulators,” *Phys. Rev. Research* **2**, 033521 (2020).
- ³⁶ C. A. Li, B. Fu, Z. A. Hu, J. Li, and S. Q. Shen, “Topological phase transitions in disordered electric quadrupole insulators,” *Phys. Rev. Lett.* **125**, 166801 (2020).
- ³⁷ Y. B. Yang, K. Li, L. M. Duan, and Y. Xu, “Higher-order topological anderson insulators,” *Phys. Rev. B* **103**, 085408 (2021).
- ³⁸ S. Spurrier and N. R. Cooper, “Kane-mele with a twist: Quasicrystalline higher-order topological insulators with fractional mass kinks,” *Phys. Rev. Research* **2**, 033071 (2020).
- ³⁹ C. B. Hua, R. Chen, B. Zhou, and D. H. Xu, “Higher-order topological insulator in a dodecagonal quasicrystal,” *Phys. Rev. B* **102**, 241102 (2020).
- ⁴⁰ A. Agarwala, V. Juričić, and B. Roy, “Higher-order topological insulators in amorphous solids,” *Phys. Rev. Research* **2**, 012067 (2020).
- ⁴¹ J. H. Wang, Y. B. Yang, N. Dai, and Y. Xu, “Structural-disorder-induced second-order topological insulators in three dimensions,” *Phys. Rev. Lett.* **126**, 206404 (2021).
- ⁴² C. Peng, R. Q. He, and Z. Y. Lu, “Correlation effects in quadrupole insulators: A quantum monte carlo study,” *Phys. Rev. B* **102**, 045110 (2020).
- ⁴³ K. Kudo, T. Yoshida, and Y. Hatsugai, “Higher-order topological mott insulators,” *Phys. Rev. Lett.* **123**, 196402 (2019).
- ⁴⁴ P. L. Zhao, X. B. Qiang, H. Z. Lu, and X. C. Xie, “Coulomb instabilities of a three-dimensional higher-order topological insulator,” *Phys. Rev. Lett.* **127**, 176601 (2021).
- ⁴⁵ T. Liu, Y. R. Zhang, Q. Ai, Z. P. Gong, K. Kawabata, M. Ueda, and F. Nori, “Second-order topological phases in non-hermitian systems,” *Phys. Rev. Lett.* **122**, 076801 (2019).
- ⁴⁶ X. W. Luo and C. W. Zhang, “Higher-order topological corner states induced by gain and loss,” *Phys. Rev. Lett.* **123**, 073601 (2019).
- ⁴⁷ H. Liu, J. K. Zhou, B. L. Wu, Z. Q. Zhang, and H. Jiang, “Real-space topological invariant and higher-order topological anderson insulator in two-dimensional non-hermitian systems,” *Phys. Rev. B* **103**, 224203 (2021).
- ⁴⁸ H. P. Hu, B. Huang, E. Zhao, and W. V. Liu, “Dynamical singularities of floquet higher-order topological insulators,” *Phys. Rev. Lett.* **124**, 057001 (2020).
- ⁴⁹ B. Huang and W. V. Liu, “Floquet higher-order topological insulators with anomalous dynamical polarization,” *Phys. Rev. Lett.* **124**, 216601 (2020).
- ⁵⁰ J. Pan and L. Zhou, “Non-Hermitian Floquet second order topological insulators in periodically quenched lattices,” *Phys. Rev. B* **102**, 094305 (2020).
- ⁵¹ A. K. Ghosh, G. C. Paul, and A. Saha, “Higher order topological insulator via periodic driving,” *Phys. Rev. B* **101**, 235403 (2020).
- ⁵² A. K. Ghosh, T. Nag, and A. Saha, “Systematic generation of the cascade of anomalous dynamical first- and higher-order modes in floquet topological insulators,” *Phys. Rev. B* **105**, 115418 (2022).
- ⁵³ T. Nag, V. Juričić, and B. Roy, “Hierarchy of higher-order floquet topological phases in three dimensions,” *Phys. Rev. B* **103**, 115308 (2021).
- ⁵⁴ A. K. Ghosh, T. Nag, and A. Saha, “Dynamical construction of quadrupolar and octupolar topological superconductors,” *Phys. Rev. B* **105**, 155406 (2022).

- ⁵⁵ I. Garate, “Phonon-induced topological transitions and crossovers in dirac materials,” *Phys. Rev. Lett.* **110**, 046402 (2013).
- ⁵⁶ M. M. Möller, G. A. Sawatzky, M. Franz, and M. Berciu, “Type-II dirac semimetal stabilized by electron-phonon coupling,” *Nat. Commun.* **8**, 2267 (2017).
- ⁵⁷ D. González-Cuadra, P. R. Grzybowski, A. Dauphin, and M. Lewenstein, “Strongly correlated bosons on a dynamical lattice,” *Phys. Rev. Lett.* **121**, 090402 (2018).
- ⁵⁸ G. Antonius and S. G. Louie, “Temperature-induced topological phase transitions: Promoted versus suppressed nontrivial topology,” *Phys. Rev. Lett.* **117**, 246401 (2016).
- ⁵⁹ L. M. Cangemi, A. S. Mishchenko, N. Nagaosa, V. Cataudella, and G. De Filippis, “Topological quantum transition driven by charge-phonon coupling in the haldane chern insulator,” *Phys. Rev. Lett.* **123**, 046401 (2019).
- ⁶⁰ H. L. Calvo, J. S. Luna, V. Dal Lago, and L. E. F. Foa Torres, “Robust edge states induced by electron-phonon interaction in graphene nanoribbons,” *Phys. Rev. B* **98**, 035423 (2018).
- ⁶¹ S. Chaudhary, A. Haim, Y. Peng, and G. Refael, “Phonon-induced floquet topological phases protected by space-time symmetries,” *Phys. Rev. Research* **2**, 043431 (2020).
- ⁶² J. Medina Dueñas, H. L. Calvo, and L. E. F. Foa Torres, “Copropagating edge states produced by the interaction between electrons and chiral phonons in two-dimensional materials,” *Phys. Rev. Lett.* **128**, 066801 (2022).
- ⁶³ Y. F. Ren, Z. H. Qiao, and Q. Niu, “Engineering corner states from two-dimensional topological insulators,” *Phys. Rev. Lett.* **124**, 166804 (2020).
- ⁶⁴ D. Sénéchal, D. Perez, and D. Plouffe, “Cluster perturbation theory for hubbard models,” *Phys. Rev. B* **66**, 075129 (2002).
- ⁶⁵ B. Sbierski and C. Karrasch, “Topological invariants for the haldane phase of interacting su-schrieffer-heeger chains: Functional renormalization-group approach,” *Phys. Rev. B* **98**, 165101 (2018).
- ⁶⁶ M. Ezawa, “Valley-polarized metals and quantum anomalous hall effect in silicene,” *Phys. Rev. Lett.* **109**, 055502 (2012).
- ⁶⁷ A. Marrazzo, M. Gibertini, D. Campi, N. Mounet, and N. Marzari, “Prediction of a large-gap and switchable Kane-Mele quantum spin hall insulator,” *Phys. Rev. Lett.* **120**, 117701 (2018).
- ⁶⁸ J.-A. Yan, S.-P. Gao, R. Stein, and G. Coard, “Tuning the electronic structure of silicene and germanene by biaxial strain and electric field,” *Phys. Rev. B* **91**, 245403 (2015).
- ⁶⁹ J. P. Hague and C. MacCormick, “Quantum simulation of electron-phonon interactions in strongly deformable materials,” *New J. Phys.* **14**, 033019 (2012).
- ⁷⁰ J. P. Mendonca and K. Jachymski, “Quantum simulation of extended electron-phonon coupling models in a hybrid rydberg atom setup,” arXiv:2208.11473 (2022).
- ⁷¹ J. Knörzer, T. Shi, E. Demler, and J. I. Cirac, “Spin-Holstein models in trapped-ion systems,” *Phys. Rev. Lett.* **128**, 120404 (2022).